

UC Berkeley

UC Berkeley Previously Published Works

Title

Systems Analysis of NADH Dehydrogenase Mutants Reveals Flexibility and Limits of *Pseudomonas taiwanensis* VLB120's Metabolism.

Permalink

<https://escholarship.org/uc/item/7pv130dp>

Journal

Applied and Environmental Microbiology, 86(11)

ISSN

0099-2240

Authors

Nies, Salome C
Dinger, Robert
Chen, Yan
[et al.](#)

Publication Date

2020-05-19

DOI

10.1128/aem.03038-19

Peer reviewed

1 **A systems analysis of NADH dehydrogenase mutants reveals flexibility and limits**
2 **of *Pseudomonas taiwanensis* VLB120's metabolism**

3 Salome C. Nies¹, Robert Dinger², Yan Chen³, Gossa G. Wordofa⁴, Mette Kristensen⁴,
4 Konstantin Schneider⁴, Jochen Büchs², Christopher J. Petzold^{3,5}, Jay D. Keasling^{3,4,5,6,7,8,}
5 ^{9,10}, Lars M. Blank^{1*}, Birgitta E. Ebert^{1,11,12}

6
7 ¹iAMB-Institute of Applied Microbiology, ABBt-Aachen Biology and Biotechnology, RWTH
8 Aachen University, Aachen, DE

9 ²AVT – Biochemical Engineering, RWTH Aachen University, Aachen, DE

10 ³Joint BioEnergy Institute, Emeryville, CA 94608, USA.

11 ⁴Novo Nordisk Foundation Center for Biosustainability, Technical University of Denmark,
12 DK-2800 Lyngby, DK

13 ⁵Lawrence Berkeley National Laboratory, Biological Systems and Engineering Division,
14 Berkeley, CA 94720, USA.

15 ⁶Virtual Institute of Microbial Stress and Survival, Lawrence Berkeley National Laboratory,
16 Berkeley, CA 94720, USA

17 ⁷Physical Biosciences Division, Lawrence Berkeley National Laboratory, Berkeley, CA
18 94720, USA

19 ⁸Dept. of Bioengineering, University of California, Berkeley, CA 94720, USA

20 ⁹Dept. of Chemical Engineering, University of California, Berkeley, CA 94720, USA

21 ¹⁰Synthetic Biochemistry Center, Institute for Synthetic Biology, Shenzhen Institutes for
22 Advanced Technologies, Shenzhen, China

23 ¹¹Australian Institute for Bioengineering and Nanotechnology (AIBN), the University of
24 Queensland, Brisbane, QLD 4072, Australia

25 ¹²CSIRO Future Science Platform in Synthetic Biology, Commonwealth Scientific and
26 Industrial Research Organisation (CSIRO), Black Mountain, ACT 2601, Australia

27

28 * Corresponding author

29

30 **Running title: NADH dehydrogenase deficiency in *P. taiwanensis***

31 **Keywords** *Pseudomonas*; NADH dehydrogenase; respiratory activity; oxidative stress;
32 electron transport chain

33

34 **Abstract**

35 Obligate aerobic organisms rely on a functional electron transport chain for energy
36 conservation and NADH oxidation. Because of this essential requirement, the genes of
37 this pathway are likely constitutively and highly expressed to avoid a cofactor imbalance
38 and energy shortage under fluctuating environmental conditions. We here investigated
39 the essentiality of the three NADH dehydrogenases of the respiratory chain of the obligate
40 aerobe *Pseudomonas taiwanensis* VLB120 and the impact of the knockouts of
41 corresponding genes on its physiology and metabolism. While a mutant lacking all three
42 NADH dehydrogenases seemed to be nonviable, the generated single or double
43 knockout strains displayed no, or only a weak, phenotype. Only the mutant deficient in
44 both type-2 dehydrogenases showed a clear phenotype with biphasic growth behavior
45 and a strongly reduced growth rate in the second phase. In-depth analyses of the
46 metabolism of the generated mutants including quantitative physiological experiments,
47 transcript analysis, proteomics, and enzyme activity assays revealed distinct responses
48 to type-2 and type-1 dehydrogenase deletions. An overall high metabolic flexibility
49 enables *P. taiwanensis* to cope with the introduced genetic perturbations and maintain
50 stable phenotypes, likely by re-routing of metabolic fluxes. This metabolic adaptability has
51 implications for biotechnological applications. While the phenotypic robustness is
52 favorable in large-scale applications with inhomogeneous conditions, the possible
53 versatile redirecting of carbon fluxes upon genetic interventions can thwart metabolic
54 engineering efforts.

55

56 **Importance**

57 While *Pseudomonas* has the capability for high metabolic activity and the provision of
58 reduced redox cofactors important for biocatalytic applications, exploitation of this
59 characteristic might be hindered by high, constitutive activity of and, consequently,

60 competition with the NADH dehydrogenases of the respiratory chain. The in-depth
61 analysis of NADH dehydrogenase mutants of *Pseudomonas taiwanensis* VLB120
62 presented here, provides insight into the phenotypic and metabolic response of this strain
63 to these redox metabolism perturbations. The observed great metabolic flexibility needs
64 to be taken into account for rational engineering of this promising biotechnological
65 workhorse towards a host with controlled and efficient supply of redox cofactors for
66 product synthesis.

67

68 **Introduction**

69 Many industrially relevant molecules, e.g., ethanol, butanediol or isoprene, are more
70 reduced than the industrially-used sugars glucose and sucrose or alternative, upcoming
71 carbon sources such as xylose or glycerol (1-3). The microbial production of those
72 favored compounds hence is inherently redox limited, i.e., by the supply of reduced redox
73 cofactors, generally NADH or NADPH. This bottleneck has been overcome in some
74 cases, e.g., 1,4 butanediol and 1,3-propanediol production in *Escherichia coli* (4, 5) or L-
75 lysine synthesis in *Corynebacterium glutamicum* (6). The strategies applied optimized the
76 host metabolism by metabolic engineering (4, 7, 8) or adapted the process conditions by
77 (co-)feeding reduced substrates (9), applying microaerobic conditions or using
78 nongrowing cells with reduced competition and cellular demand for the redox cofactor
79 (10-13). Alternatively, microorganisms can be applied that naturally outperform the
80 classic, industrial workhorses with respect to redox cofactor supply. Pseudomonads are
81 outstanding in this regard as they exhibit a driven-by-demand phenotype, which allows
82 them to strongly enforce the metabolic activity under stress conditions with increased
83 energy demand, reported to result in a more than 2-fold carbon uptake rate and an even
84 8-fold increase of the NAD(P)H regeneration rate relative to standard growth conditions
85 (12, 14, 15). This behavior holds great promise for using this species for the bioproduction
86 of highly reduced chemicals such as phenol, (S)-styrene oxide, rhamnolipids, and methyl
87 ketones (16-20). Yet, competition is high as the NAD⁺/NADH couple functions as a
88 coenzyme in over 300 oxidation/reduction reactions (21). *Pseudomonas* strains without
89 apparent fermentative metabolism are obligate aerobes that rely on constitutive activity
90 of the NADH dehydrogenases to ensure adequate oxidation of NADH to NAD⁺. Hence,
91 we argue here that a naturally high NADH oxidation activity might impair the effective
92 fueling of production pathways with reducing equivalents. We here set out to provide an
93 in-depth analysis of the redox metabolism of *Pseudomonas taiwanensis* VLB120, a

94 strictly aerobic bacterium, focusing on the role and essentiality of the individual NADH
95 dehydrogenases for NADH oxidation and energy conservation.

96 While the mammalian mitochondrial electron transport chain constitutes only NADH
97 dehydrogenase type-1, a multi-subunit enzyme referred to as Nuo or complex 1 (22),
98 which couples the electron transfer to proton translocation and hence contributes to ATP
99 generation (23), aerobic bacteria have developed diverse NADH oxidation capabilities
100 linked to the respiratory chain. Besides, the Nuo complex, most species possess one to
101 two isozymes of the non-proton translocating type-2 dehydrogenase (Ndh), also termed
102 alternative NADH dehydrogenase, which transfers electrons from NADH to ubiquinone
103 but does not contribute to the membrane potential (23, 24). In some species a third
104 sodium pumping type-3 dehydrogenase (Nqr) can be found. As with the facultative
105 aerobic yeast *Saccharomyces cerevisiae*, several bacteria lack the Nuo complex and only
106 possess a type-2 dehydrogenases or are reported to mainly rely on the activity of this
107 enzyme for NADH re-oxidation (25, 26). Likewise, the genome of *P. taiwanensis* VLB120
108 encodes two types of NADH dehydrogenases, type-1 (EC 7.1.1.2) and two isoforms of
109 type-2 (EC 1.6.99.3). Type-1 is encoded by the genes PVLB_15600-15660 designated
110 as the *nuo* operon. The two type-2 NADH dehydrogenases are encoded by PVLB_13270
111 and PVLB_21880, designated as *ndh1* and *ndh2*, respectively. Ndh1 and Ndh2, both
112 consist of a single polypeptide chain.

113 In the present study, NADH dehydrogenase mutants of *P. taiwanensis* VLB120 were
114 generated and characterized regarding growth, respiratory activity, and transcriptional
115 and proteomic changes to elucidate the impact of redox metabolism perturbation on the
116 cellular physiology.

117 **Results**

118 **NADH dehydrogenase activity is vital for *P. taiwanensis* but single enzymes of the**
119 **redundant oxidation system are dispensable.**

120 The NADH dehydrogenase type-1 operon encoded by *nuoA-N* (PVLB_15600-15660) and
121 the two type-2 NADH dehydrogenases encoded by *ndh1* (PVLB_13270) and *ndh2*
122 (PVLB_21880) were successfully deleted from the *P. taiwanensis* VLB120 genome using
123 the I-SceI-based pEMG plasmid (27). The double knockout mutants $\Delta\Delta ndh$ and
124 $\Delta nuo\Delta ndh1$ were successfully obtained, however, several attempts failed to generate the
125 double knockout of Δnuo and $\Delta ndh2$. All gene deletions were confirmed by Sanger
126 sequencing. The five NADH-dehydrogenase mutants demonstrated that the NADH
127 dehydrogenases, Nuo, Ndh1, and Ndh2 are not essential individually. While the presence
128 of either Nuo or Ndh2 is sufficient to sustain the viability of *P. taiwanensis* VLB120, Ndh1
129 seems to be unable to compensate for the loss of Nuo and Ndh2. Similarly, it has been
130 reported that single deletions of NADH dehydrogenases in *P. aeruginosa* PAO1 did not
131 result in a growth defect or decrease in NADH oxidation activity, whereas in the double
132 ($\Delta nuoI\Delta ndh$) and triple knockout ($\Delta nuoI\Delta ndh\Delta nqrA-F$) the NADH oxidation activity was
133 abolished (28). Concludingly, Nuo and Ndh account for the total NADH dehydrogenase
134 activity in this *Pseudomonas* strain. Note that *P. aeruginosa* is a facultative anaerobe able
135 to respire on nitrate and ferment pyruvate while *P. taiwanensis* VLB120 does not possess
136 the necessary enzymatic makeup.

137 A likewise total loss of NADH dehydrogenase activity in the obligate aerobic
138 *P. taiwanensis* VLB120 strain seems to be lethal indicating that the strain relies on the
139 presence of these dehydrogenases for NADH oxidation and that alternative, native NADH
140 consuming reactions do not suffice to efficiently re-oxidize this vital cofactor under the
141 tested conditions.

142 **The $\Delta\Delta ndh$ mutant exhibits a growth-phase dependent growth defect**

143 *P. taiwanensis* VLB120 and the five NADH dehydrogenase deletion strains $\Delta ndh1$,
144 $\Delta ndh2$, $\Delta\Delta ndh$, Δnuo , and $\Delta nuo\Delta ndh1$ were characterized for growth, glucose utilization,
145 CO₂ formation, and oxygen consumption in batch shake-flask experiments. The single
146 NADH-dehydrogenase type-2 mutants, $\Delta ndh1$ and $\Delta ndh2$, showed the same growth and

147 sugar co-utilization profile as the wild type *P. taiwanensis* VLB120 (Figure 1A, B, and C).
148 The loss of the megaplasmid pSTY during NADH dehydrogenase deletions resulted in a
149 growth advantage for the generated mutants, which was determined to result in a 14 %
150 higher growth rate for *P. taiwanensis* VLB120 pSTY⁻ compared to the pSTY⁺ wild type
151 (29). For a comparison of mutants and wild type, the growth rate of the wild type was
152 corrected accordingly and is referred to as $\mu_{\text{recalc.}}$.

153 While the single gene deletion mutants $\Delta ndh1$ and $\Delta ndh2$ showed a wild-type physiology
154 (Figure 1, Table 1), the type-2 double mutant $\Delta\Delta ndh$ reproducibly showed two growth
155 phases (Figure 1D). After wild type-like growth in the first phase, the growth rate dropped
156 drastically in the second growth phase. Interestingly, the strong decrease in the growth
157 rate (~86 %) was not correlated with an equal reduction of the carbon uptake, which
158 showed a decrease of only ~38 %.

159 *Pseudomonas* can catabolize glucose either via the phosphorylative or the oxidative
160 pathway. In the latter, a membrane-bound glucose dehydrogenase (*gcd*) oxidizes
161 periplasmic glucose to gluconate coupled with the reduction of pyrroloquinoline quinone
162 (PQQ). The phosphorylative pathway starts in the cytoplasm with the phosphorylation of
163 glucose to glucose-6-phosphate catalyzed by the glucokinase (Glk) (30, 31).

164 The mutant $\Delta\Delta ndh$ showed a significant increase in the specific gluconate yield in the
165 early exponential growth phase. The same behavior was observed in the Δnuo and
166 $\Delta nuo\Delta ndh1$ mutants (Table 1).

167 Besides the characterization for growth and glucose consumption, the respiratory
168 behavior of the wild type and NADH dehydrogenase mutants was studied (Figure 2,
169 Supplementary Figure S1). Again, only the $\Delta\Delta ndh$ mutant showed a different phenotype
170 characterized by a stagnating oxygen transfer rate (OTR) after 6 hours (Figure 2B). This
171 change in the OTR development is an indication for substrate inhibition, here, potentially
172 by NADH, which cannot be oxidized at the rate required for fast growth. The onset of the

173 reduced specific oxygen uptake rate also correlated well with the change of the growth
174 rate (Figure 1D).

175 During growth on glucose, the respiratory quotient (RQ), defined as the ratio of OTR and
176 CTR, is generally close to one (32, 33). Due to the oxidation of glucose to gluconate in
177 the periplasm of *Pseudomonas* strains, the measured OTR for all tested mutants during
178 the first 6 hours of cultivation was higher than the CTR resulting in an RQ below 1 (Figure
179 2A, Supplementary Figure S1). Indeed, the surplus of consumed oxygen, calculated from
180 the sectional integrals between the OTR and CTR ($\int OTR dt - \int CTR dt$), correlated with
181 the produced gluconate (Table 1, Figure 2A). During glucose conversion, roughly half of
182 the overall consumed oxygen was used for the oxidation of glucose to gluconate and the
183 re-oxidation of the reduced PQQ formed by the glucose dehydrogenase activity.
184 Consequently, in the glucose phase, the cells can partially uncouple glucose oxidation
185 and energy provision from NADH formation, relieving the dependence on NADH
186 dehydrogenase activity. The O₂ and CO₂ transfer rate (CTR) of $\Delta ndh2$ and $\Delta\Delta ndh$
187 (Supplementary Figure S1) showed a double peak, which occurred in the same time
188 frame as glucose depletion, and, hence, might be due to the diauxic shift from glucose to
189 gluconate. We assume that the diauxic shift also occurred in the other strains but was not
190 recorded by the measurement frequency of three measurements per hour. The
191 respiratory coefficient on gluconate was close to one for all *Pseudomonas* strains,
192 indicating that no products other than biomass and CO₂ were formed during catabolism
193 of this substrate.

194 **NADH dehydrogenase gene deletions affect expression levels but do not result in** 195 **altered *in vitro* NADH oxidation activities**

196 To further elucidate the NADH oxidation activity in the different mutants, and hence, the
197 importance of the three NADH dehydrogenases for oxidizing NADH and fueling the
198 electron transport chain, we performed *in vitro* NADH oxidation assays. Inverted

199 membrane vesicles were prepared at early-, mid-, and late-exponential growth phase,
200 and the NADH oxidation rate was determined from the decrease in absorbance at 340 nm
201 over time. Note that the SDS PAGE of the membrane fraction showed up to 21 prominent
202 protein bands (data not shown). Therefore, we cannot exclude the presence of further
203 membrane-bound NADH-dependent enzymes, e.g., the transhydrogenase PntAB, which
204 might have contributed to the measured NADH oxidation rate. However, there is a high
205 probability that the NADH oxidation is very specific for NADH dehydrogenases as most
206 NADH-dependent enzymes, e.g., alcohol or aldehyde dehydrogenase, require electron
207 acceptors other than O₂. Additional experiments with alternative electron acceptors have
208 not been performed. In the early-exponential growth phase, in which none of the strains
209 showed a growth defect, all single mutants possessed NADH oxidation activities at levels
210 similar to the wild type of around 1.2 U mg protein⁻¹ (Table 4), which is in the range of *in*
211 *vitro* rates reported for other organisms (34). Overall, the NADH oxidation rate was rather
212 stable in all mutants, indicating high metabolic flexibility of *P. taiwanensis* VLB120 to
213 maintain redox homeostasis.

214 To further substantiate this hypothesis, we examined potential changes at the
215 transcriptional level by qPCR on samples taken in the early, mid-, and late-exponential
216 growth phase. HPLC analysis showed that glucose and/or gluconate were still left when
217 sampling the late-exponential growth phase, i.e., the cells were still metabolically active
218 (data not shown). The fold changes were normalized against the wild type in the
219 corresponding growth phase. The single and double deletions of the type-2 NADH
220 dehydrogenase encoding genes (Figure 3A-C) had only minor effects (fold change < 2)
221 on the remaining NADH dehydrogenase gene expression. While the type-1 deletions
222 strains, Δnuo and $\Delta nuo\Delta ndh1$, showed a substantial upregulation of the *ndh2* gene
223 expression (Figure 3D-E). The expression of the *ndh1* gene in both the Δnuo and
224 $\Delta nuo\Delta ndh1$ was unaffected; we only observed a small increase for mutant Δnuo in the

225 early growth phase. This finding suggests that *ndh2* is probably the only NADH
226 dehydrogenase gene that is regulated in response to the cellular NADH/NAD⁺ ratio. The
227 consequent essentiality would further explain why the double deletion of *nuo* and *ndh2*
228 was lethal. The observation that $\Delta\Delta ndh$ is only growth impaired during mid- to late-
229 exponential growth indicates that either the Nuo complex is less active in these phases
230 or that the PQQ-dependent glucose dehydrogenase activity during the early growth phase
231 enables sufficient ATP synthesis independent of NADH dehydrogenase activity.

232 **Double deletion of the type-2 NADH dehydrogenases affect intracellular redox** 233 **cofactor levels**

234 We found that the NADH oxidation rate was not or only slightly compromised by the
235 introduced gene deletions but that the *ndh2* level was significantly upregulated,
236 suggesting that its expression is controlled by the redox state of the cell. Moreover, even
237 though we performed the *in vitro* enzyme assay with a physiological meaningful NADH
238 concentration of 125 μ M (35) to mimic *in vivo* conditions, we cannot exclude differences
239 between the actual *in vivo* NADH dehydrogenase activities of the mutants as the redox
240 cofactor levels might have been altered.

241 For that reason, we determined the intracellular abundance of NADH and NAD⁺ in the
242 early-, mid-, and late-exponential growth phase. Since the two single mutants of type-2
243 had no growth phenotype and showed no apparent changes on the transcriptional level,
244 we restricted the analysis to the two double mutants and single *nuo* deletion mutant Δnuo ,
245 $\Delta\Delta ndh$, and $\Delta nuo\Delta ndh1$.

246 The $\Delta nuo\Delta ndh1$ showed a higher NADH/NAD⁺ ratio in the late-exponential growth phase
247 but also a high variability in the triplicate experiments curtailing the statistical significance.
248 The double mutant $\Delta\Delta ndh$ had a significantly increased NADH/NAD⁺ ratio in the mid- and
249 late-exponential growth phase compared to the wild type (Figure 4). This significantly
250 increased NADH/NAD⁺ ratio in $\Delta\Delta ndh$ probably triggered the observed drop in the growth
251 rate in the mid-exponential phase, e.g., because of a potential inhibition of the Nuo

252 complex. To prove this hypothesis, we overexpressed the water-forming NADH oxidase
253 (Nox) from *Streptococcus pneumoniae* (36). Nox is known to be very specific for NADH,
254 unable to oxidize NADPH and has been described to produce no toxic hydrogen peroxide
255 (37). The enzyme activity hence solely results in NADH oxidation and is suitable to
256 elucidate the effect of relief from NADH accumulation. The overexpression of *nox* did not
257 restore the wild type phenotype but we observed a higher respiratory activity in mutant
258 $\Delta\Delta ndh$ Nox⁺ in comparison to mutant $\Delta\Delta ndh$ (Supplementary Figure S3). In contrast to
259 the response of *P. putida* KT2440, Nox activity in $\Delta\Delta ndh$ did not lead to a decrease in
260 growth rate or biomass yield (14, 38).

261 **Proteomics analysis reveals re-routing of the carbon flux in the $\Delta\Delta ndh$ mutant**

262 We further performed shotgun proteomics analysis to explain possible metabolic changes
263 in early-, mid-, and late-exponential growth phase in *P. taiwanensis* VLB120 due to NADH
264 dehydrogenase deletions. The relative quantitative data were used to categorize the
265 detected proteins into three groups: (1) significantly upregulated or (2) downregulated
266 proteins (fold change > 2, adjusted p-value < 0.05), and (3) weak/no effect proteins (fold
267 change < 2). The proteins were further grouped into functional categories according to
268 the KEGG database classification (39), e.g., transport, carbohydrate metabolism, amino
269 acid metabolism (Supplementary Table S 2). The most strongly represented categories
270 are summarized in Figure 5.

271 Per the physiological and transcript data, we did not observe significant changes in the
272 proteome for either NADH dehydrogenase type-2 single mutants ($\Delta ndh1$: 9 of 24 proteins
273 significantly up/downregulated, $\Delta ndh2$: 8 of 36 proteins significantly up/downregulated;
274 Figure 5, Supplementary Table S2, Supplementary File S3). Proteomic changes in both
275 type-1 mutants (Δnuo : 50 of 139 proteins significantly up-/downregulated, $\Delta nuo\Delta ndh1$: 60
276 of 165 proteins significantly up-/downregulated) were more significant compared to the
277 type-2 single-gene knockout mutants and very similar to each other (Figure 5). The
278 double deletion mutant $\Delta\Delta ndh$ showed more alterations in the proteome in the early- and

279 late-exponential phase (17 and 37 of 107 proteins significantly up-/downregulated) than
280 in the mid-exponential phase (2 significantly up-/downregulated proteins) (Figure 5 and
281 Supplementary Table S2).

282 In the following paragraphs, we are focusing on changes observed in the $\Delta\Delta ndh$ mutant
283 for proteins related to carbon uptake, energy generation, and oxidative stress response
284 and are highlighting distinct differences to the type-1 NADH dehydrogenase mutants.

285 The OprB-I porin (PVLB_20075), a carbohydrate selective porin, and the D-gluconate
286 transporter GntT (PVLB_13665) located in the outer and inner membrane, respectively,
287 were higher increased in the $\Delta\Delta ndh$ mutant during the early- and late-exponential growth
288 phase, while the glucokinase quantity was strongly reduced in all growth phases. These
289 data suggest that $\Delta\Delta ndh$ oxidized glucose via glucose dehydrogenase (Gcd) to gluconate
290 to a greater extent than the wild type. In contrast, the quantity of OprB-I in the type-1
291 NADH dehydrogenase mutants during the later growth phase was decreased. This
292 change might, however, be explained by the faster glucose depletion in these mutants
293 (Figure 1).

294 During the late-exponential growth of the $\Delta\Delta ndh$ mutant, all enzymes of the arginine
295 deiminase (ADI) pathway were more strongly expressed while they were significantly
296 downregulated in the NADH dehydrogenase type-1 mutants (Table 6). This pathway
297 catalyzes a three-step conversion of arginine to ornithine, ammonium, and carbon dioxide
298 coupled to ATP generation (40). Likewise, the isocitrate lyase (AceA), the first enzyme of
299 the glyoxylate shunt, was upregulated in the $\Delta\Delta ndh$ mutant but downregulated in the Δnuo
300 mutant, which instead showed a slight upregulation of the 2-oxoglutarate dehydrogenase
301 complex of the TCA cycle during mid- and late-exponential growth. These changes
302 indicate that the mutant $\Delta\Delta ndh$ used the glyoxylate shunt and not exclusively the TCA
303 cycle in the late-exponential growth phase.

304 We further observed remarkable changes in proteins combating oxidative stress. While
305 deletion of the *nuo* operon (Δnuo and $\Delta nuo\Delta ndh1$) resulted in a generally reduced
306 abundance of proteins involved in the oxidative stress response, those mutants deficient
307 in one of the two type-2 dehydrogenases displayed increased levels of peroxidases and
308 peroxiredoxin proteins. The abundance of the catalase-peroxidase KatG was strongly
309 decreased in both type-1 mutants, whereas it was weakly increased in the $\Delta\Delta ndh$ mutant.
310 Additionally, only the peroxidase encoded by PP_0235 and the quinone reductase ChrR
311 were more highly expressed in the $\Delta\Delta ndh$ mutant with the latter being reported to be
312 induced by superoxide (41) while peroxiredoxin AhpC was weakly upregulated in the
313 single-gene deletion mutants, $\Delta ndh1$ and $\Delta ndh2$ (Supplementary File S3). These findings
314 indicate that the deletion of both type-2 dehydrogenases increases oxidative stress. We
315 determined ROS formation in *P. taiwanensis* VLB120 and mutant $\Delta\Delta ndh$ using the ROS-
316 sensitive dye H₂-DCFA (2',7'-dichlorodihydrofluorescein diacetate), which is oxidized by
317 ROS to fluorescent DCF. Indeed, we observed an increase in ROS formation in $\Delta\Delta ndh$
318 concomitant with the reduction in growth (Supplementary Figure S2) underlining the
319 proteomics results and strengthening our hypothesis.

320 Discussion

321 The presented in-depth analysis of NADH dehydrogenase mutants revealed high
322 metabolic robustness of *P. taiwanensis* VLB120 to a partial loss of the three NADH
323 dehydrogenases, but also the essentiality of residual NADH dehydrogenase activity, as
324 the simultaneous deficiency of Nuo and Ndh2 was lethal likely due to inefficient NADH
325 oxidation or ATP provision.

326 In accordance with the observed phenotypic robustness of most mutants, *in vitro* NADH
327 oxidation activities in the mutant strains were not reduced. While this can be explained
328 for those mutants deficient in the *nuo* operon with a significant upregulation of *ndh2*, no
329 transcriptional changes of NADH dehydrogenase related genes were observed for the

330 other mutants. In contrast, the mutant with Nuo as the sole NADH dehydrogenase
331 ($\Delta\Delta ndh$) showed a growth phenotype in the mid-exponential growth phase. While the *in*
332 *vitro* NADH oxidation capacity was not altered, several changes in protein and metabolite
333 levels were observed. We have summarized our current model of the potential underlying
334 metabolic changes in Figure 6. The wild type-like growth of the $\Delta\Delta ndh$ mutant on glucose
335 is likely sustained by periplasmic glucose oxidation to gluconate instead of
336 phosphorylation, which partially uncouples the oxidation of the carbon source from NADH
337 formation. The increased gluconate yield of the $\Delta\Delta ndh$ mutant underlines this hypothesis.
338 The monitored respiratory activity and the match of gluconate accumulation and surplus
339 oxygen consumption emphasize that no side products other than gluconate were
340 produced to sustain the wild type-like growth. *In vitro* studies have shown the formation
341 of reactive oxygen species (ROS) such as superoxide ($O_2^{\cdot-}$) and hydrogen peroxide
342 (H_2O_2) by enzymes of the electron transport chain due to electron leakage to oxygen.
343 Cells activate antioxidant defense system to combat ROS, which can result in severe cell
344 damage or even death. Nuo (complex I) and cytochrome bc1 (complex III) are considered
345 the main sites for ROS in mitochondria and *P. fluorescens* (42, 43) but rather the type-2
346 dehydrogenase in *E. coli*, which does not possess complex III (44). It has further been
347 reported that an oversupply of NADH can enhance ROS production (45, 46).
348 The observed ROS accumulation in $\Delta\Delta ndh$ during mid-exponential growth phase might,
349 hence, be either due to an increased Nuo activity relative to the wild type or the elevated
350 NADH/NAD⁺ ratio. In line with this hypothesis, it has been shown that *M. tuberculosis*
351 NADH dehydrogenase mutants with a similarly elevated NADH/NAD⁺ ratio were more
352 susceptible to (additional) oxidative stress than those with a lower NADH/NAD⁺ ratio (47).
353 ROS induced stress but also a potential NADH inhibition of metabolic enzymes might
354 further explain the reduced growth and respiratory activity. However, while the latter

355 increased upon *nox* expression, Nox mediated NADH oxidation did not restore growth,
356 indicating that further limitations remained.

357 The activation of the glyoxylate shunt in $\Delta\Delta ndh$, as indicated by the proteome data, might
358 contribute to stress reduction in two ways. Firstly, this shortcut of the TCA cycle bypasses
359 NAD(P)H-producing steps (48-50). For *Pseudomonas putida* KT2440, the production of
360 a surplus of NADPH during growth on glucose has been reported (51) and it was
361 speculated that the excess NADPH is converted to NADH by the transhydrogenase
362 PntAB, which has been shown to be expressed in this strain under similar growth
363 conditions (38). Assuming PntAB transhydrogenase activity in *P. taiwanensis*, which is
364 equipped with the respective genes, attenuated NADP⁺ reduction would, hence, result in
365 an overall reduced NADH formation. Secondly, the glyoxylate formed by the isocitrate
366 lyase AceA activity, which was upregulated in $\Delta\Delta ndh$, can react with hydrogen peroxide
367 to produce formate and CO₂ (48, 52). This ROS combating strategy has been reported
368 for *Pseudomonas aeruginosa*, *Burkholderia cenocepacia*, and *Staphylococcus aureus*,
369 even though *S. aureus* has no functional glyoxylate shunt (48, 53-55). Note, however,
370 that neither higher formate dehydrogenase abundance nor formate accumulation was
371 observed in the $\Delta\Delta ndh$ mutant.

372 The deletion of *nuo* and the accompanied higher Ndh2 activity did not result in a similar
373 stress response, which is in accordance with corresponding *M. tuberculosis* mutants (47).
374 A probable energy shortage due to reduced respiratory activity might have been
375 counteracted by ATP generation via the ADI pathway, which seems to be activated in
376 $\Delta\Delta ndh$ according to the proteome data. This pathway generates 1 mol ATP per mol
377 arginine (40, 56) and was described to be activated upon energy depletion in lactic
378 bacteria (57) and Pseudomonads, e.g., in *P. putida* DOT-T1E under energy-demanding
379 solvent stress conditions (58, 59) and in *P. aeruginosa* under oxygen limiting conditions
380 (40).

381 In this study, we showed high metabolic flexibility of *P. taiwanensis* VLB120 to
382 interventions in the redox metabolism, which confers robust phenotypic behavior by a
383 possible re-routing of metabolic fluxes. This metabolic adaptability and phenotypic
384 robustness can be advantageous for biocatalysis but simultaneously be challenging
385 because it impedes the prediction of mutant behavior and can lever out metabolic
386 engineering efforts. Hence, to effectively turn this promising microbe into a controllable,
387 biotechnological workhorse, further systems biological and physiological analyses, such
388 as ¹³C-metabolic flux analysis, are needed.

389 **Materials and Methods**

390 **Strains, media and culture conditions**

391 Bacterial strains used in this study are listed in Table 4. Strains were propagated in
392 Lysogeny Broth (LB) containing 10 g L⁻¹ peptone, 5 g L⁻¹ sodium chloride, and 5 g L⁻¹
393 yeast extract (60). Cetrimide agar (Sigma-Aldrich, St. Louis, MO, USA) was used after
394 mating procedures to select for *Pseudomonas*. Growth and characterization experiments
395 were performed using mineral salt medium (MSM) (61) containing 3.88 g L⁻¹ K₂HPO₄,
396 1.63 g L⁻¹ NaH₂PO₄, 2 g L⁻¹ (NH₄)₂SO₄, 0.1 g L⁻¹ MgCl₂·6H₂O, 10 mg L⁻¹ EDTA, 2 mg L⁻¹
397 ZnSO₄·7 H₂O, 1 mg L⁻¹ CaCl₂·2H₂O, 5 mg L⁻¹ FeSO₄·7 H₂O, 0.2 mg L⁻¹ Na₂MoO₄·2H₂O,
398 0.2 mg L⁻¹ CuSO₄·5 H₂O, 0.4 mg L⁻¹ CoCl₂·6 H₂O, 1 mg L⁻¹ MnCl₂·2 H₂O supplemented
399 with 25 mM glucose. For the preparation of solid LB, 1.5 % agar was added to the
400 medium. For plasmid maintenance and in the gene deletion procedure, antibiotics were
401 added to the medium as required. Gentamycin and kanamycin were used at
402 concentrations of 25 mg L⁻¹ and 50 mg L⁻¹, respectively. Because of the leaky expression
403 of *nox* from plasmid pS2311, *P. taiwanensis* VLB120 strains bearing plasmid
404 pS2311 were grown without the addition of the inducer cyclohexanone.
405 Batch flask experiments were performed in 50 mL medium in 500-mL flasks under oxic
406 conditions on a horizontal rotary shaker with a throw of 50 mm and frequency of 300 rpm.

407 *E. coli* was grown at 37 °C, *Pseudomonas* at 30 °C. The chemicals used in this work were
408 obtained from Carl Roth (Karlsruhe, Germany), Sigma-Aldrich (St. Louis, MO, USA), or
409 Merck (Darmstadt, Germany) unless stated otherwise. The main cultures were inoculated
410 from liquid pre-cultures to an approximate OD_{600nm} of 0.05. All experiments were
411 performed in biological triplicates unless stated otherwise.

412 **Plasmid cloning and generation of deletion strains**

413 Genomic DNA of *P. taiwanensis* VLB120 was isolated using the High Pure PCR Template
414 Preparation Kit (Hoffmann-La-Roche, Basel, Switzerland). Upstream (TS1) and
415 downstream (TS2) regions with a length of 400-800 bp flanking the specific target gene
416 were amplified using Q5 High-Fidelity Polymerase (New England Biolabs, Ipswich, MA,
417 USA). Primers were ordered as unmodified DNA Oligonucleotides from Eurofins
418 Genomics (Ebersberg, Germany) and are listed in Table S5. The suicide delivery vector
419 pEMG was isolated using the NEB Monarch Plasmid Miniprep Kit (New England Biolabs,
420 Ipswich, MA, USA). The isolated plasmid was digested with restriction enzymes
421 purchased from New England Biolabs (Ipswich, MA, USA). For plasmid construction,
422 Gibson Assembly using NEB Builder Hifi DNA Assembly (New England Biolabs, Ipswich,
423 MA, USA) was used. Plasmids were transformed into electrocompetent *E. coli* DH5α λpir1
424 via electroporation (62). Transformants and chromosomally engineered *Pseudomonas*
425 were screened by colony PCR using OneTaq 2x Master Mix (New England Biolabs,
426 Ipswich, MA, USA). The cell material was lysed in alkaline polyethylene glycol for
427 enhanced colony PCR efficiency as described previously (63).

428 Targeted gene deletions were performed using the I-SceI-based system developed by
429 Martinez-Garcia and de Lorenzo (27). The conjugational transfer of the mobilizable
430 knock-out plasmids from *E. coli* DH5α λpir1 to *Pseudomonas* was performed via
431 triparental patch mating (16). After conjugation, the pSW-2 plasmid encoding the I-SceI-
432 endonuclease was conjugated into *Pseudomonas* co-integrates. The addition of 3-
433 methylbenzoate for the induction of I-SceI expression was omitted as the basal

434 expression level was sufficient. Kanamycin-selective clones were directly isolated,
435 positive clones were cured of pSW-2 and restreaked several times. The gene deletion
436 was confirmed by colony PCR and Sanger sequencing. No complementation studies
437 were performed because for it has been shown the I-SceI scarless gene deletion method
438 we used that the double strand breaks do not result in random mutations. Moreover the
439 method does not introduce foreign DNA material making side effects very unlikely.

440 **Analytical methods**

441 The optical density of cell suspensions was measured at a wavelength of 600 nm using
442 an Ultrospec 10 spectrophotometer (GE Healthcare, Chicago, IL, USA). The cell dry
443 weight (CDW) was calculated by multiplying OD_{600nm} with a gravimetrically determined
444 correlation factor of 0.39. For HPLC analysis the samples were centrifuged at 17,000 x g
445 for 5 min and the supernatant was stored at -20°C until further analysis.

446 Glucose and gluconate concentrations were measured by high-performance liquid
447 chromatography using a Beckman System Gold 126 Solvent Module equipped with a
448 System Gold 166 UV-detector (Beckman Coulter) and a Smartline RI detector 2300
449 (KNAUER Wissenschaftliche Geräte, Berlin, Germany). Analytes were separated on the
450 organic resin column Metab AAC (ISERA, Düren, Germany) eluted with 5 mM H_2SO_4 at
451 an isocratic flow of 0.6 mL min^{-1} at 40 °C for 20 min. Glucose and gluconate were
452 analyzed using the RI detector whereas gluconate was determined with the UV detector
453 at a wavelength of 210 nm.

454 **Proteomic profiling of NADH dehydrogenase mutants**

455 Samples for proteome profiling were taken during early-, mid-, and late-exponential
456 growth at an OD_{600nm} of 0.5, 2.5, and after depletion of glucose, checked with test strips
457 for rapid detection of glucose (Medi-Test, Macherey-Nagel, Düren, Germany),
458 respectively. Proteins were extracted from cell biomass and subsequently prepared for
459 shotgun proteomic experiments as described previously (64). All samples were analyzed
460 on an Agilent 6550 iFunnel Q-TOF mass spectrometer (Agilent Technologies, Santa

461 Clara, CA) coupled to an Agilent 1290 UHPLC system. Twenty (20) μg of peptides were
462 separated on a Sigma–Aldrich Ascentis Peptides ES-C18 column (2.1 mm \times 100 mm, 2.7
463 μm particle size, operated at 60°C) at a 0.400 mL min^{-1} flow rate and eluted with the
464 following gradient: initial condition was 95 % solvent A (0.1 % formic acid) and 5 % solvent
465 B (99.9 % acetonitrile, 0.1 % formic acid). Solvent B was increased to 35 % over 120 min,
466 and then increased to 50 % over 5 min, then up to 90 % over 1 min, and held for 7 min at
467 a flow rate of 0.6 mL min^{-1} , followed by a ramp back down to 5 % B over 1 min where it
468 was held for 6 min to re-equilibrate the column to original conditions. Peptides were
469 introduced to the mass spectrometer from the LC by using a Jet Stream source (Agilent
470 Technologies) operating in positive-ion mode (3,500 V). Source parameters employed
471 gas temp (250°C), drying gas (14 L min^{-1}), nebulizer (35 psig), sheath gas temp (250°C),
472 sheath gas flow (11 L min^{-1}), VCap (3,500 V), fragmentor (180 V), OCT 1 RF Vpp (750
473 V). The data were acquired with Agilent MassHunter Workstation Software, LC/MS Data
474 Acquisition B.06.01 operating in Auto MS/MS mode whereby the 20 most intense ions
475 (charge states, 2–5) within 300–1,400 m/z mass range above a threshold of 1,500 counts
476 were selected for MS/MS analysis. MS/MS spectra (100–1,700 m/z) were collected with
477 the quadrupole set to “medium” resolution and were acquired until 45,000 total counts
478 were collected or for a maximum accumulation time of 333 ms. Former parent ions were
479 excluded for 0.1 min following MS/MS acquisition. The acquired data were exported as
480 mgf files and searched against the pan proteome that is highly related to *Pseudomonas*
481 *taiwanensis* VLB120 with Mascot search engine version 2.3.02 (Matrix Science). The
482 resulting search results were filtered and analyzed by Scaffold v 4.3.0 (Proteome
483 Software Inc.). The normalized spectral counts of each sample were exported from
484 Scaffold, and the relative quantity changes of identified proteins in mutant samples were
485 calculated in comparison to the wild type sample. The statistical significance of these
486 changes and the adjusted p-values were evaluated by limma R package. The mass

487 spectrometry proteomics data have been deposited to the ProteomeXchange Consortium
488 via the PRIDE (65) partner repository with the dataset identifier PXD013623 and
489 10.6019/PXD013623.

490 **RNA preparation and analysis**

491 Samples for transcription analysis were taken during early-, mid- and late-exponential
492 growth at an OD_{600nm} of approximately 0.5, approximately 2.5 and after glucose depletion,
493 respectively. Prior to RNA isolation, the culture sample was diluted with the DNA/RNA
494 protection reagent of the Monarch Total RNA Miniprep Kit (New England Biolabs, Ipswich,
495 MA, USA), followed mechanical lysis with ZR BashingBead™ Lysis Tube (0.5mm) (Zymo
496 Research, Irvine, CA, USA) for 1 min using the Mini-Beadbeater-16 (Biospec, Bartlesville,
497 OK, USA). After a centrifugation step at 16,000 x g for 2 min the supernatant was
498 transferred into a new tube. An equal volume of RNA lysis buffer of the Monarch Total
499 RNA Miniprep Kit was added, and the RNA isolation was continued as described in the
500 supplier's manual. After the last elution step, an additional in-tube DNase treatment was
501 done using RNase-free DNaseI (New England Biolabs, Ipswich, MA, USA). The final RNA
502 yield and purity were evaluated by the absorption ratio A_{260}/A_{280} measured with a
503 Nanodrop (Thermo Scientific, Rockford, IL, USA). The synthesis of cDNA for reverse
504 transcription was carried out with a Protoscript II first strand cDNA synthesis kit (New
505 England Biolabs, Ipswich, MA, USA) using 120 ng total RNA and 60 μM random
506 hexamers. The qPCR analyses were conducted with 5 μL of the reverse transcription
507 reaction mixture with gene-specific primers (Supplementary Table S1) and the Luna
508 Universal qPCR Master Mix (New England Biolabs, Ipswich, MA, USA) was used. Primers
509 for qPCR were designed with the PrimerQuest Tool of IDT technologies. Gene expression
510 levels for each individual sample were normalized relative to the internal reference gene,
511 *rpoB* and the wild type in the corresponding growth phase calculated by a mathematical
512 method based on the calculated real-time PCR efficiencies (66). The qPCR was

513 performed with the CFX96 Real-Time PCR Detection System (Biorad, Hercules, CA,
514 USA). All qPCR reactions were performed in triplicates.

515 **Inverted membrane vesicle preparation and NADH oxidation activity**

516 Cultures were harvested at early-exponential growth phase at an optical density (OD_{600nm})
517 of approximately 0.5, as well as in the late-exponential growth phase (OD_{600nm} , of 3-4).

518 Inverted membrane vesicles were prepared as described by Borisov (67). Briefly, cells
519 were centrifuged for 8 min at 5,000 x g and resuspended in 2 mL spheroplast buffer (200
520 mM Tris-HCl pH 8.0, 2 mM EDTA, 30 % sucrose), centrifuged again and resuspended in
521 1 mL spheroplast buffer. Spheroplasts were prepared using lysozyme (0.03 g) and
522 incubated for 30 min at room temperature. Spheroplasts were centrifuged for 10 min at
523 5,000 x g and resuspended in 2 mL sonication buffer (100 mM HEPES-KOH pH 7.5, 50
524 mM K_2SO_4 , 10 mM $MgSO_4$, 2 mM DTT, 0.5 mM PMSF). The vesicles were sonicated
525 (Bioruptor, Diadenode, Belgium) in 4 cycles à 30 sec at high intensity with an intermediate
526 pause of 30 sec in ice water. The inverted membrane vesicles were centrifuged twice for
527 10 min at 5,000 x g to remove cell debris. The supernatant was centrifuged for 30 min at
528 120,000 x g and the resulting pellet was resuspended in the assay buffer (25 mM HEPES,
529 25 mM BIS-TRIS propane pH 7, 10 mM $MgSO_4$).

530 The freshly prepared inverted membrane vesicles were immediately used for the
531 determination of the NADH oxidation activity as we observed a rapid activity decline when
532 the membrane samples were stored on ice. 150 $\mu L mL^{-1}$ isolated membrane fractions
533 were added to the assay buffer, and the reaction was initiated by the addition of 125 μM
534 NADH. The total volume of the assay was 200 μL . The NADH oxidation was monitored
535 over 30 min at 340 nm in a Synergy™ MX microplate reader (BioTek, Winooski, VT, USA).
536 For calculating the specific enzyme activity, we used the NADH molar extinction
537 coefficient $\epsilon_{NADH} = 6.22 \text{ mM}^{-1} \text{ cm}^{-1}$; one unit of activity was the quantity that catalyzed the
538 oxidation of 1 μmol of NADH per min. The protein concentration was measured with the

539 reducing agent compatible Pierce BCA Protein Assay Kit (Thermo Scientific, Rockford,
540 IL, USA).

541 **Respiration activity monitoring**

542 The cultivations and measurements of the oxygen transfer rate (OTR) and the carbon
543 dioxide transfer rate (CTR) were performed in a modified RAMOS System, developed by
544 the Chair of Biochemical Engineering (RWTH Aachen University) (33, 68). The standard
545 RAMOS for shake flasks is commercially available from the Kühner AG (Birsfelden,
546 Switzerland) or HiTec Zang GmbH (Herzogenrath, Germany). All cultivations were
547 performed in 250-mL Ramos flasks with 10 % (v/v) filling volume using MSM medium
548 supplemented with 25 mM glucose. The cultures were inoculated from liquid pre-cultures
549 to an approximate OD_{600nm} of 0.05. The OTR and CTR were measured thrice per hour.
550 All experiments were performed in biological duplicates.

551 **Redox cofactor quantification**

552 Samples for redox cofactor analysis were collected from early-, mid-, and late-exponential
553 growth phase at OD_{600nm} of approximately 0.6, 2.2, and 4.0, respectively. The samples
554 were rapidly transferred into 15-mL Falcon tubes containing 5 mL of quenching solution
555 (acetonitrile:methanol:water, 40:40:20, v/v) with ¹³C labeled cell extracts at -40°C. After
556 three freeze-thaw cycles, the samples were centrifuged at 13,000 x g for 5 min and
557 concentrated by evaporating the quenching solvent using a vacuum concentrator
558 (SAVANT, SpeedVac, Thermo Fisher Scientific, San Diego, CA, USA) for 5 hours
559 followed by lyophilization (LABCONCO, FreeZone, Kansas City, MO, USA). All dried
560 extracts were stored -80°C until analysis or re-suspended in LC-MS grade water for LC-
561 MS analysis. All redox cofactor metabolites were measured on an AB SCIEX Qtrap1 5500
562 mass spectrometer (AB SCIEX, Framingham, MA, USA) operated in negative ion and
563 selected multiple reaction monitoring (MRM) mode. The column XSELECT HSS XP (150
564 mm × 2.1 mm × 2.5 μm) (Waters, Milford, MA, USA) with ion-pairing technique was used
565 for the chromatography separation as previously described (69). Peak integration and

566 metabolite quantification were performed using an isotope-ratio-based approach on Multi-
567 Quant™ 3.0.2 (AB SCIEX) software as previously described (70, 71).

568 **ROS assay**

569 The ROS sensitive fluorescent dye 2',7'-dichlorodihydrofluorescein diacetate (H₂-DCFA,
570 Sigma Aldrich, St. Louis, MO, USA) was used to monitor the ROS formation in
571 *P. taiwanensis* VLB120. Cells were harvested at multiple time points during the growth
572 experiment and centrifuged for 5 min at 8,000 x g. The pellet was washed once in the
573 mineral salt medium described above but lacking nitrogen (MSM-N) and centrifuged
574 again. The cells were resuspended to an optical density of OD_{600nm} of ~0.4 in 1 mL MSM-
575 N but supplemented with 25 mM glucose to allow respiratory activity. The ROS-sensitive
576 H₂-DCFA dye was added to the cells to a final concentration of 20 μM. The cells were
577 incubated in the dark for 30 min at 30°C at 250 rpm for aeration. After the incubation, the
578 cells were immediately analyzed in the microplate reader Synergy™ MX (BioTek,
579 Winooski, VT, USA). The oxidized fluorescent DCF was measured using Ex/Em 504/529
580 nm. The measurement was performed in biological and technical triplicates. As a positive
581 control, 1 mM H₂O₂ was included in all experiments and treated in the same way as the
582 biological samples (data not shown).

583

584 **Acknowledgments**

585 This study has been conducted within the ERA SynBio project SynPath (Grant ID
586 031A459) with financial support of the German Federal Ministry of Education and
587 Research and is part of the Joint BioEnergy Institute, supported by the Office of Science,
588 Office of Basic Energy Sciences and Office of Biological and Environmental Research of
589 the U.S. Department of Energy under Contract No. DE-AC02-05CH11231. BEE and SCN
590 acknowledge financial support by the German Academic Exchange Service (DAAD)
591 through the thematic network Aachen-California Network of Academic Exchange
592 (ACalNet) funded by the German Federal Ministry of Education and Research (BMBF).
593 BEE acknowledges partial support by the CSIRO-UQ Synthetic Biology Alliance. LMB
594 acknowledges funding by the Cluster of Excellence "The Fuel Science Center - Adaptive
595 Conversion Systems for Renewable Energy and Carbon Sources" (EXC 2186), which is
596 funded by the Excellence Initiative of the German federal and state governments to
597 promote science and research at German universities. We thank Stephani Baum and
598 Uwe Conrath for sharing lab equipment and for technical support. We are grateful to Itay
599 Budin for discussions and instruction on the membrane isolation and *in vitro* assays and
600 Sophia Nölting for support with qPCR measurements. We thank Benedikt Wynands and
601 Nick Wierckx for sharing the strain *P. taiwanensis* VLB120 pSTY⁻, Victor de Lorenzo
602 (Centro Nacional de Biotecnología - CNB, Madrid) for providing plasmid pEMG, and
603 Pablo Nikel for providing plasmid pS2311-Nox.

604

605 References

- 606 1. Kracke F, Kromer JO. 2014. Identifying target processes for microbial electrosynthesis by
607 elementary mode analysis. *BMC Bioinformatics* 15:410.
- 608 2. Kohler KA, Blank LM, Frick O, Schmid A. 2015. D-Xylose assimilation via the Weimberg
609 pathway by solvent-tolerant *Pseudomonas taiwanensis* VLB120. *Environ Microbiol*
610 17:156-70.
- 611 3. Becker J, Lange A, Fabarius J, Wittmann C. 2015. Top value platform chemicals: bio-based
612 production of organic acids. *Curr Opin Biotechnol* 36:168-175.
- 613 4. Yim H, Haselbeck R, Niu W, Pujol-Baxley C, Burgard A, Boldt J, Khandurina J, Trawick JD,
614 Osterhout RE, Stephen R, Estadilla J, Teisan S, Schreyer HB, Andrae S, Yang TH, Lee SY,
615 Burk MJ, Van Dien S. 2011. Metabolic engineering of *Escherichia coli* for direct production
616 of 1,4-butanediol. *Nat Chem Biol* 7:445.
- 617 5. Nakamura CE, Whited GM. 2003. Metabolic engineering for the microbial production of
618 1,3-propanediol. *Curr Opin Biotechnol* 14:454-459.
- 619 6. Takeno S, Murata R, Kobayashi R, Mitsuhashi S, Ikeda M. 2010. Engineering of
620 *Corynebacterium glutamicum* with an NADPH-generating glycolytic pathway for L-lysine
621 production. *Appl Environ Microbiol* 76:7154-60.
- 622 7. Fasan R, Crook NC, Peters MW, Meinhold P, Buelter T, Landwehr M, Cirino PC, Arnold FH.
623 2011. Improved product-per-glucose yields in P450-dependent propane
624 biotransformations using engineered *Escherichia coli*. *Biotechnol Bioeng* 108:500-10.
- 625 8. Becker J, Zelder O, Häfner S, Schröder H, Wittmann C. 2011. From zero to hero--design-
626 based systems metabolic engineering of *Corynebacterium glutamicum* for L-lysine
627 production. *Metab Eng* 13:159-68.
- 628 9. Berríos-Rivera SJ, Bennett GN, San K-Y. 2002. Metabolic Engineering of *Escherichia coli*:
629 increase of NADH availability by overexpressing an NAD⁺-dependent formate
630 dehydrogenase. *Metab Eng* 4:217-229.
- 631 10. Jain R, Huang J, Yuan Q, Yan Y. 2015. Engineering microaerobic metabolism of *E. coli* for
632 1,2-propanediol production. *J Ind Microbiol Biotechnol* 42:1049-55.
- 633 11. Blank LM, Ebert BE, Buhler B, Schmid A. 2008. Metabolic capacity estimation of
634 *Escherichia coli* as a platform for redox biocatalysis: constraint-based modeling and
635 experimental verification. *Biotechnol Bioeng* 100:1050-65.
- 636 12. Blank LM, Ionidis G, Ebert BE, Bühler B, Schmid A. 2008. Metabolic response of
637 *Pseudomonas putida* during redox biocatalysis in the presence of a second octanol phase.
638 *FEBS J* 275:5173-5190.
- 639 13. Julsing MK, Kuhn D, Schmid A, Bühler B. 2012. Resting cells of recombinant *E. coli* show
640 high epoxidation yields on energy source and high sensitivity to product inhibition.
641 *Biotechnol Bioeng* 109:1109-1119.
- 642 14. Ebert BE, Kurth F, Grund M, Blank LM, Schmid A. 2011. Response of *Pseudomonas putida*
643 KT2440 to increased NADH and ATP demand. *Appl Environ Microbiol* 77:6597-6605.
- 644 15. Rühl J, Schmid A, Blank LM. 2009. Selected *Pseudomonas putida* strains able to grow in
645 the presence of high butanol concentrations. *Appl Environ Microbiol* 75:4653-4656.
- 646 16. Wynands B, Lenzen C, Otto M, Koch F, Blank LM, Wierckx N. 2018. Metabolic engineering
647 of *Pseudomonas taiwanensis* VLB120 with minimal genomic modifications for high-yield
648 phenol production. *Metab Eng* 47:121-133.
- 649 17. Wierckx NJP, Ballerstedt H, Bont JaMD, Wery J. 2005. Engineering of solvent-tolerant
650 *Pseudomonas putida* S12 for bioproduction of phenol from glucose. *Appl Environ*
651 *Microbiol* 71:8221-8227.

- 652 18. Tiso T, Sabelhaus P, Behrens B, Wittgens A, Rosenau F, Hayen H, Blank LM. 2016. Creating
653 metabolic demand as an engineering strategy in *Pseudomonas putida* – rhamnolipid
654 synthesis as an example. *Metab Eng Commun* 3:234-244.
- 655 19. Dong J, Chen Y, Benites VT, Baidoo EEK, Petzold CJ, Beller HR, Eudes A, Scheller HV, Adams
656 PD, Mukhopadhyay A, Simmons BA, Singer SW. 2019. Methyl ketone production by
657 *Pseudomonas putida* is enhanced by plant-derived amino acids. *Biotechnol Bioeng*
658 doi:10.1002/bit.26995.
- 659 20. Park JB, Bühler B, Panke S, Witholt B, Schmid A. 2007. Carbon metabolism and product
660 inhibition determine the epoxidation efficiency of solvent-tolerant *Pseudomonas sp.*
661 strain VLB120ΔC. *Biotechnol Bioeng* 98:1219-29.
- 662 21. Foster JW, Park YK, Penfound T, Fenger T, Spector MP. 1990. Regulation of NAD
663 metabolism in *Salmonella typhimurium*: molecular sequence analysis of the bifunctional
664 *nadR* regulator and the *nadA-pnuC* operon. *J Bacteriol* 172:4187-96.
- 665 22. Spehr V, Schlitt A, Scheide D, Guénebaut V, Friedrich T. 1999. Overexpression of the
666 *Escherichia coli nuo*-operon and isolation of the overproduced NADH:ubiquinone
667 oxidoreductase (complex I). *Biochemistry* 38:16261-16267.
- 668 23. Pruss BM, Nelms JM, Park C, Wolfe AJ. 1994. Mutations in NADH:ubiquinone
669 oxidoreductase of *Escherichia coli* affect growth on mixed amino acids. *J Bacteriol*
670 176:2143-50.
- 671 24. Matsushita K, Ohnishi T, Kaback HR. 1987. NADH-ubiquinone oxidoreductases of the
672 *Escherichia coli* aerobic respiratory chain. *Biochemistry* 26:7732-7737.
- 673 25. Melo AMP, Bandejas TM, Teixeira M. 2004. New Insights into Type II NAD(P)H:Quinone
674 Oxidoreductases. *Microbiol Mol Biol Rev* 68:603.
- 675 26. Spero MA, Aylward FO, Currie CR, Donohue TJ. 2015. Phylogenomic Analysis and
676 Predicted Physiological Role of the Proton-Translocating NADH:Quinone Oxidoreductase
677 (Complex I) Across Bacteria. *mBio* 6:e00389-15.
- 678 27. Martínez-García E, de Lorenzo V. 2011. Engineering multiple genomic deletions in Gram-
679 negative bacteria: Analysis of the multi-resistant antibiotic profile of *Pseudomonas putida*
680 KT2440. *Environ Microbiol* 13:2702-2716.
- 681 28. Torres A, Kasturiarachi N, DuPont M, Cooper VS, Bomberger J, Zemke A. 2019. NADH
682 dehydrogenases in *Pseudomonas aeruginosa* growth and virulence. *Front Microbiol* 10.
- 683 29. Wynands B, Otto M, Runge N, Preckel S, Polen T, Blank LM, Wierckx N. 2019. Streamlined
684 *Pseudomonas taiwanensis* VLB120 chassis strains with improved bioprocess features. *ACS*
685 *Synth Biol* 8:2036-2050.
- 686 30. Vicente M, Canovas JL. 1973. Glucolysis in *Pseudomonas putida*: physiological role of
687 alternative routes from the analysis of defective mutants. *J Bacteriol* 116:908-14.
- 688 31. del Castillo T, Ramos JL, Rodriguez-Herva JJ, Fuhrer T, Sauer U, Duque E. 2007. Convergent
689 peripheral pathways catalyze initial glucose catabolism in *Pseudomonas putida*: genomic
690 and flux analysis. *J Bacteriol* 189:5142-52.
- 691 32. Jeude M, Dittrich B, Niederschulte H, Anderlei T, Knocke C, Klee D, Büchs J. 2006. Fed-
692 batch mode in shake flasks by slow-release technique. *Biotechnol Bioeng* 95:433-45.
- 693 33. Anderlei T, Zang W, Papaspyrou M, Büchs J. 2004. Online respiration activity
694 measurement (OTR, CTR, RQ) in shake flasks. *Biochem Eng J* 17:187-194.
- 695 34. Calhoun MW, Gennis RB. 1993. Demonstration of separate genetic loci encoding distinct
696 membrane-bound respiratory NADH dehydrogenases in *Escherichia coli*. *J Bacteriol*
697 175:3013-9.
- 698 35. Bennett BD, Kimball EH, Gao M, Osterhout R, Van Dien SJ, Rabinowitz JD. 2009. Absolute
699 metabolite concentrations and implied enzyme active site occupancy in *Escherichia coli*.
700 *Nat Chem Biol* 5:593-9.

- 701 36. Akkaya Ö, Pérez-Pantoja DR, Calles B, Nickel PI, de Lorenzo V. 2018. The metabolic redox
702 regime of *Pseudomonas putida* tunes its evolvability toward novel xenobiotic substrates.
703 mBio 9:e01512-18.
- 704 37. Yu J, Bryant AP, Marra A, Lonetto MA, Ingraham KA, Chalker AF, Holmes DJ, Holden D,
705 Rosenberg M, McDevitt D. 2001. Characterization of the *Streptococcus pneumoniae*
706 NADH oxidase that is required for infection. Microbiology 147:431-8.
- 707 38. Nickel PI, Pérez-Pantoja D, de Lorenzo V. 2016. Pyridine nucleotide transhydrogenases
708 enable redox balance of *Pseudomonas putida* during biodegradation of aromatic
709 compounds. Environ Microbiol 18:3565-3582.
- 710 39. Kanehisa M, Sato Y, Kawashima M, Furumichi M, Tanabe M. 2016. KEGG as a reference
711 resource for gene and protein annotation. Nucleic Acids Res 44:D457-62.
- 712 40. Mercenier A, Simon JP, Vander Wauven C, Haas D, Stalon V. 1980. Regulation of enzyme
713 synthesis in the arginine deiminase pathway of *Pseudomonas aeruginosa*. J Bacteriol
714 144:159-163.
- 715 41. Gonzalez CF, Aekerley DF, Lynch SV, Martin A. 2005. ChrR, a soluble quinone reductase of
716 *Pseudomonas putida* that defends against H₂O₂. J Biol Chem 280:22590-22595.
- 717 42. Mailloux RJ, Lemire J, Appanna VD. 2011. Metabolic networks to combat oxidative stress
718 in *Pseudomonas fluorescens*. Antonie Van Leeuwenhoek 99:433-42.
- 719 43. Imlay JA. 2003. Pathways of oxidative damage. Annu Rev Microbiol 57:395-418.
- 720 44. Messner KR, Imlay JA. 1999. The identification of primary sites of superoxide and
721 hydrogen peroxide formation in the aerobic respiratory chain and sulfite reductase
722 complex of *Escherichia coli*. J Biol Chem 274:10119-28.
- 723 45. Murphy MP. 2009. How mitochondria produce reactive oxygen species. Biochem J 417:1-
724 13.
- 725 46. Vinogradov AD, Grivennikova VG. 2016. Oxidation of NADH and ROS production by
726 respiratory complex I. Biochim Biophys Acta 1857:863-71.
- 727 47. Vilcheze C, Weinrick B, Leung LW, Jacobs WR, Jr. 2018. Plasticity of *Mycobacterium*
728 *tuberculosis* NADH dehydrogenases and their role in virulence. Proc Natl Acad Sci U S A
729 115:1599-1604.
- 730 48. Ahn S, Jung J, Jang IA, Madsen EL, Park W. 2016. Role of glyoxylate shunt in oxidative
731 stress response. J Biol Chem 291:11928-38.
- 732 49. Kornberg HL. 1966. The role and control of the glyoxylate cycle in *Escherichia coli*.
733 Biochem J 99:1-11.
- 734 50. Lemire J, Alhasawi A, Appanna VP, Tharmalingam S, Appanna VD. 2017. Metabolic
735 defence against oxidative stress: the road less travelled so far. J Appl Microbiol 123:798-
736 809.
- 737 51. Kohlstedt M, Wittmann C. 2019. GC-MS-based ¹³C metabolic flux analysis resolves the
738 parallel and cyclic glucose metabolism of *Pseudomonas putida* KT2440 and *Pseudomonas*
739 *aeruginosa* PAO1. Metab Eng 54:35-53.
- 740 52. Thomas SC, Alhasawi A, Auger C, Omri A, Appanna VD. 2016. The role of formate in
741 combatting oxidative stress. Antonie Van Leeuwenhoek 109:263-71.
- 742 53. Van Acker H, Sass A, Bazzini S, De Roy K, Udine C, Messiaen T, Riccardi G, Boon N, Nelis
743 HJ, Mahenthalingam E, Coenye T. 2013. Biofilm-grown *Burkholderia cepacia* complex
744 cells survive antibiotic treatment by avoiding production of reactive oxygen species. PLoS
745 One 8:e58943.
- 746 54. Somerville GA, Proctor RA. 2009. At the crossroads of bacterial metabolism and virulence
747 factor synthesis in *Staphylococci*. Microbiol Mol Biol Rev 73:233-48.

- 748 55. Somerville GA, Said-Salim B, Wickman JM, Raffel SJ, Kreiswirth BN, Musser JM. 2003.
749 Correlation of acetate catabolism and growth yield in *Staphylococcus aureus*: implications
750 for host-pathogen interactions. *Infect Immun* 71:4724-32.
- 751 56. Thauer RK, Jungermann K, Decker K. 1977. Energy conservation in chemotrophic
752 anaerobic bacteria. *Bacteriol Rev* 41:100-180.
- 753 57. Fernández M, Zúñiga M. 2006. Amino acid catabolic pathways of lactic acid bacteria. *Crit*
754 *Rev Microbiol* 32:155-183.
- 755 58. Segura A, Godoy, P., van Dillewijn, P., Hurtado, A., Arroyo, N., Santacruz, S., Ramos, J.-L.
756 2005. Proteomic analysis reveals the participation of energy- and stress-related proteins
757 in the response of *Pseudomonas putida* DOT-T1E to toluene *J Bacteriol* 187:5937-5945.
- 758 59. Ramos JL, Duque E, Rodriguez-Herva JJ, Godoy P, Haidour A, Reyes F, Fernandez-Barrero
759 A. 1997. Mechanisms for solvent tolerance in bacteria. *J Biol Chem* 272:3887-90.
- 760 60. Sambrook J, E.F. Fritsch, and T. Maniatis. 1982. *Molecular cloning: A laboratory manual*.
761 Cold Spring Harbour Press.
- 762 61. Hartmans S, Smits JP, van der Werf MJ, Volkering F, de Bont JA. 1989. Metabolism of
763 Styrene Oxide and 2-Phenylethanol in the Styrene-Degrading Xanthobacter Strain 124X.
764 *Appl Environ Microbiol* 55:2850-5.
- 765 62. Choi KH, Kumar A, Schweizer HP. 2006. A 10-min method for preparation of highly
766 electrocompetent *Pseudomonas aeruginosa* cells: application for DNA fragment transfer
767 between chromosomes and plasmid transformation. *J Microbiol Methods* 64:391-7.
- 768 63. Chomczynski P, Rymaszewski M. 2006. Alkaline polyethylene glycol-based method for
769 direct PCR from bacteria, eukaryotic tissue samples, and whole blood. *BioTechniques*
770 40:454, 456, 458.
- 771 64. Gonzalez Fernandez-Nino SM, Smith-Moritz AM, Chan LJ, Adams PD, Heazlewood JL,
772 Petzold CJ. 2015. Standard flow liquid chromatography for shotgun proteomics in
773 bioenergy research. *Front Bioeng Biotechnol* 3:44.
- 774 65. Perez-Riverol Y, Csordas A, Bai J, Bernal-Llinares M, Hewapathirana S, Kundu DJ, Inuganti
775 A, Griss J, Mayer G, Eisenacher M, Perez E, Uszkoreit J, Pfeuffer J, Sachsenberg T, Yilmaz
776 S, Tiwary S, Cox J, Audain E, Walzer M, Jarnuczak AF, Ternent T, Brazma A, Vizcaino JA.
777 2019. The PRIDE database and related tools and resources in 2019: improving support for
778 quantification data. *Nucleic Acids Res* 47:D442-D450.
- 779 66. Pfaffl MW. 2001. A new mathematical model for relative quantification in real-time RT-
780 PCR. *Nucleic Acids Res* 29:e45.
- 781 67. Borisov VB, Murali R, Verkhovskaya ML, Bloch Da, Han H, Gennis RB, Verkhovsky MI. 2011.
782 Aerobic respiratory chain of *Escherichia coli* is not allowed to work in fully uncoupled
783 mode. *Proc Natl Acad Sci U S A* 108:17320-4.
- 784 68. Schulte A, Schilling JV, Nolten J, Korona A, Krömke H, Vennekötter J-B, Schillheim B,
785 Wessling M, Conrath U, Büchs J. 2018. Parallel online determination of ethylene release
786 rate by Shaken Parsley cell cultures using a modified RAMOS device. *BMC Plant Biol*
787 18:101.
- 788 69. McCloskey D, Utrilla J, Naviaux RK, Palsson BO, Feist AM. 2015. Fast Swinnex filtration
789 (FSF): a fast and robust sampling and extraction method suitable for metabolomics
790 analysis of cultures grown in complex media. *Metabolomics* 11:198-209.
- 791 70. Wu L, Mashego MR, van Dam JC, Proell AM, Vinke JL, Ras C, van Winden WA, van Gulik
792 WM, Heijnen JJ. 2005. Quantitative analysis of the microbial metabolome by isotope
793 dilution mass spectrometry using uniformly ¹³C-labeled cell extracts as internal standards.
794 *Anal Biochem* 336:164-71.
- 795 71. Mashego MR, Wu L, Van Dam JC, Ras C, Vinke JL, Van Winden WA, Van Gulik WM, Heijnen
796 JJ. 2004. MIRACLE: mass isotopomer ratio analysis of U-¹³C-labeled extracts. A new

- 797 method for accurate quantification of changes in concentrations of intracellular
798 metabolites. *Biotechnol Bioeng* 85:620-628.
- 799 72. Cunin R, Glansdorff N, Piérard A, Stalon V. 1986. Biosynthesis and metabolism of arginine
800 in bacteria. *Microbiol Rev* 50:314-352.
- 801 73. Ditta G, Stanfield S, Corbin D, Helinski DR. 1980. Broad host range DNA cloning system for
802 Gram-negative bacteria: construction of a gene bank of *Rhizobium meliloti*. *Proc Nat Acad*
803 *Sci USA* 77:7347-7351.
- 804

805 **Figures legends**

806 **Figure 1.** Physiological characterization of *P. taiwanensis* VLB120 (A) and the NADH
807 dehydrogenase deficient mutants $\Delta ndh1$ (B), $\Delta ndh2$ (C), $\Delta\Delta ndh$ (D), Δnuo (E), and
808 $\Delta nuo\Delta ndh1$ (F). The strains were cultured in MSM with 25 mM glucose. The OD_{600nm}
809 (black circles), glucose (blue squares), gluconate (green triangles) were measured over
810 time. The shadowed area in (D) indicates the first growth phase. The data shown are the
811 mean of biological triplicates; error bars show the standard deviation. μ_{recalc} is the growth
812 rate of *P. taiwanensis* VLB120 pSTY⁻. The wild type OD_{600nm} are plotted (grey, open
813 circles) in graphs (B)-(F) for comparison.

814

815
816 **Figure 2.** Respiratory activity of *P. taiwanensis* VLB120 and the $\Delta\Delta ndh$ mutant. (A) CTR
817 and OTR date of the wild type strain, the highlighted area corresponds to the surplus of
818 consumed oxygen. The area was calculated from the sectional integrals between the
819 OTR (dashed line) and CTR (solid line). (B) Oxygen transfer rates (OTR, dashed line)
820 during cultivation of *P. taiwanensis* VLB120 (black) and mutant $\Delta\Delta ndh$ (green).

821

822 **Figure 3.** Relative gene expression of the NADH dehydrogenase encoding genes *ndh1*,
823 *ndh2*, and *nuoA* in NADH dehydrogenase mutants $\Delta ndh1$ (A), $\Delta ndh2$ (B), $\Delta\Delta ndh$ (C),
824 Δnuo (D), and $\Delta nuo\Delta ndh1$ (E) at early-, mid-, and late-exponential growth phase
825 normalized to the corresponding values of the wild type. mRNA abundance was
826 determined by quantitative PCR. Values were normalized to the relative transcript level
827 of *P. taiwanensis* VLB120 in the corresponding growth phase. *nuoA* was used as a proxy
828 for the expression of the *nuo* operon. Gene deletions in the respective mutant are marked
829 with 'X' and were not analyzed by qPCR. Experiments were performed in biological
830 triplicates.

831

832 **Figure 4.** Quantification of the NADH/NAD⁺ ratio in the *P. taiwanensis* VLB120 (black)
833 and the NADH dehydrogenase mutants $\Delta\Delta ndh$ (green), Δnuo (orange), and $\Delta nuo\Delta ndh1$
834 (red) in early-, mid- and late-exponential growth phase.

835

836

837 **Figure 5.** Significant changes at proteome level of *P. taiwanensis* VLB120 NADH
838 dehydrogenase mutants in early- (A), mid- (B), and late-exponential (C) growth phase
839 relative to the wild type. Proteins are clustered into functional categories according to the
840 KEGG classification system (39). Each bar represents the number of proteins in the
841 depicted category, the abundance of which was either increased or decreased in
842 response to NADH dehydrogenase deficiency. Experiments were performed in biological
843 triplicates.

844

845 **Figure 6.** Proposed metabolic changes caused by type-2 NADH dehydrogenase
846 deficiency in *P. taiwanensis* VLB120. An increased NADH/NAD⁺ ratio **(1)** might result in
847 substrate inhibition of the Nuo complex as well as ROS production **(2)**, which is
848 reported for this NADH dehydrogenase (45, 46). Re-routing of the flux through the TCA
849 cycle into the glyoxylate shunt **(3)** reduces redox cofactor formation (48-50) and helps to
850 scavenge reactive oxygen species by glyoxylate (48, 52). Limited ATP provision from
851 oxidative phosphorylation can be mitigated by upregulation of the ADI pathway, based
852 on our proteomics data **(4)** (58, 72). The light representation of the Ndh dehydrogenase
853 indicates deficiency of both isozymes. ETC, electron transport chain; ROS, reactive
854 oxygen species; ADI, arginine deiminase pathway; Nuo, type-1 NADH dehydrogenase;
855 Ndh, type-2 NADH dehydrogenase; Sdh, succinate dehydrogenase; bc1, cytochrome
856 bc1 (complex III); cbb3, cytochrome cbb3 (complex IV); QH₂, ubiquinol; Q, ubiquinone;
857 SUC, succinate, SUCCoA, succinyl-CoA; FUM, fumarate.

858

859 **Tables**

860 **Table 1.** Calculated carbon uptake, gluconate accumulation, oxygen formation rates,
 861 biomass, and the gluconate yield of wild type and NADH dehydrogenase mutants during
 862 exponential growth.

Strain	Carbon uptake rate^a	Biomass^b	Gluconate yield^c	Gluconate accumulation^d	Surplus O₂ consumption^e
	[mmol g_{CDW}⁻¹ h⁻¹]	[g L⁻¹]	[mmol g_{CDW}⁻¹]	[mM]	[mM]
wild type	7.3 ± 0.4	0.7 ± 0.0	13.7 ± 2.1	8.9 ± 1.1	9.2 ± 1.3
<i>Δndh1</i>	7.9 ± 0.2	0.7 ± 0.0	11.6 ± 1.7	8.6 ± 1.3	8.1 ± 0.1
<i>Δndh2</i>	7.2 ± 0.2	0.6 ± 0.0	12.8 ± 1.2	7.7 ± 0.3	6.3 ± 0.5
<i>ΔΔndh</i>	8.9 ± 0.5 / 3.5 ± 0.2	0.4 ± 0.0	20.7 ± 1.1	8.8 ± 0.4	7.2 ± 1.6
<i>Δnuo</i>	7.0 ± 1.2	0.6 ± 0.1	25.3 ± 2.5	14.5 ± 0.8	12.9 ± 0.2
<i>ΔnuoΔndh1</i>	6.1 ± 0.2	0.8 ± 0.0	20.9 ± 1.4	16.1 ± 1.3	14.1 ± 3.9

863 ^a For *ΔΔndh*, separate growth rates were determined for phase 1 (2-6 h) and phase 2 (6-
 864 8 h). For all other mutants, growth rates were calculated for the exponential phase
 865 (between 3-4 h to 6-7 h after inoculation).

866 ^b The biomass concentration at the time point of the monitored maximum gluconate
 867 concentration according to ^d; shown is the mean of duplicate or triplicate experiments and
 868 the corresponding standard deviation

869 ^c The gluconate yield was calculated by dividing the monitored maximum gluconate
 870 concentration according to ^d with the corresponding biomass concentration according to
 871 ^b; shown is the mean of duplicate or triplicate experiments and the corresponding
 872 standard deviation.

873 ^d The gluconate accumulation was determined from offline monitored measurements;
 874 shown is the mean of duplicate or triplicate experiments and the corresponding standard
 875 deviation.

876 ^e The surplus oxygen consumption was calculated from the sectional integrals between
 877 the OTR (mmol L⁻¹ h⁻¹) and CTR (mmol L⁻¹ h⁻¹) between start of the cultivation and the
 878 timepoint of intersection of CTR and OTR (see Figure 2); shown is the mean of duplicate
 879 experiments and the corresponding standard deviation.

880

881 **Table 2.** Specific NADH oxidation activities of inverted membrane vesicles of
 882 *P. taiwanensis* VLB120 wild type and NADH dehydrogenase mutants in the early and
 883 late-exponential growth phase.

Strain	Specific NADH oxidation activity ^a (U mg _{protein} ⁻¹)	
	Early- exponential	Late- exponential
Wild type	1.2 ± 0.2	0.7 ± 0.2
<i>Δndh1</i>	1.3 ± 0.1	0.5 ± 0.1
<i>Δndh2</i>	1.0 ± 0.2	0.4 ± 0.1
<i>ΔΔndh</i>	1.1 ± 0.1	0.5 ± 0.2
<i>Δnuo</i>	1.2 ± 0.1	0.5 ± 0.1
<i>ΔnuoΔndh1</i>	0.8 ± 0.1	0.5 ± 0.2

^a Mean values and standard deviations

were determined from independent,

biological triplicates

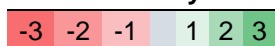
884

885 **Table 3.** Protein abundance in NADH dehydrogenase mutants relative to the wild type.

886 Proteins marked with a diamond (◊) are discussed in the text.

Gene name	Gene function or product ^a	$\Delta\Delta ndh$			Δnuo			$\Delta nuo\Delta ndh1$		
		early	mid	late	early	mid	late	early	mid	Late
Log2 fold change relative to the wild type^b										
Carbohydrate metabolism										
Pgk	Phosphoglycerate kinase									
SucC	Succinate-CoA ligase, subunit beta				0.3	0.3	0.5	0.4	0.4	0.5
SucD	Succinate-CoA ligase, subunit alpha					0.4	1.0	0.6	0.8	1.0
SdhB	Succinate dehydrogenase						0.8	0.5	0.5	0.8
◊ Glk	Glucokinase	-3.1	-2.8	-2.5						
TktA	Transketolase			-1.5						
◊ AceA	Isocitrate lyase			0.8			-1.3			
Ppc	Phosphoenolpyruvate carboxylase					1.35				
Idh	Isocitrate dehydrogenase						0.6		0.5	-2.6
◊ Gcd	Quinoprotein glucose dehydrogenase						2.2			
Energy metabolism										
TsaA	Putative peroxiredoxin					0.5	0.7	0.5	0.48	0.79
Fpr-I	Ferredoxin-NADP(+) reductase	-1.0		-1.1				-3.1	-1.7	
◊ PP_0235	Peroxidase			3.2						
◊ ChrR	Quinone reductase			2.0						
Amino acid metabolism										
◊ ArcA	Arginine deiminase			1.1			-1.9			-1.9
◊ ArcB	Ornithine carbamoyltransferase			1.2			-2.3			-2.3
◊ ArcC	Carbamate kinase			0.8	-0.6		-2.0			-1.5
Transporter/Carbon uptake										
◊ OprB-I	Porin	1.4		1.4			-2.5		-2.0	-2.8
◊ GntT	D-gluconate transporter	0.6		1.2				0.9		
GtsA	Mannose/glucose ABC transporter	0.8			0.9	0.8		1.0	0.7	
GtsD	Mannose/glucose ABC transporter	0.7								
Stress proteins										
◊ KatG	Catalase-peroxidase			0.7			-2.3			-2.8
TauA	Taurine ABC transporter			2.4						
DnaK	Chaperone protein			-0.3						
TrxA	Thioredoxin	0.9		0.6						

Color key⁸⁸⁷



Fold change⁸⁸⁹

^a Gene function assignment differs from Figure 5

890 ^b Numbers indicate the fold change for upregulated (+) and downregulated (-) proteins
 891 relative to the wild type, and the lack of a number indicates no differential production.
 892

893 **Table 4.** Bacterial strains and plasmids used in this study.

Strain	Relevant characteristics ^a	Reference
<i>E. coli</i>		
DH5α	<i>fhuA2 lac(del)U169 phoA glnV44</i> Φ80' <i>lacZ(del)M15 gyrA96 recA1</i> <i>relA1 endA1 thi-1 hsdR17</i>	NEB
DH5α λpir1	F ⁻ , Δ <i>lac</i> 169, <i>rpoS</i> (Am), <i>robA1</i> , <i>recA1uidA</i> (Δ <i>Mlul</i> :: <i>pir</i> -116; host for <i>oriV</i> (R6K) vectors in high copy number	Thermo Fisher Scientific
HB101 pRK2013	Sm ^R , <i>hsdR</i> -M+, <i>proA2</i> , <i>leuB6</i> , <i>thi-1</i> , <i>recA</i> ; bears plasmid pRK2013	(73)
DH5α pSW-2	Gm ^r , DH5α bearing pSW-2	(27)
DH5α λpir1 pEMG	Km ^r , DH5α λpir1 bearing plasmid pEMG	(27)
DH5α λpir1 pEMG_ko_ndh1	Km ^r , PVLB_13270 deletion plasmid	This study
DH5α λpir1 pEMG_ko_ndh2	Km ^r , PVLB_21880 deletion plasmid	This study
DH5α λpir1 pEMG_ko_nuo	Km ^r , PVLB_15600-15660 deletion plasmid	This study
Plasmids		
pS2311·Nox	Km ^r ; derivative of vector pSEVA2311 with the <i>nox</i> gene from <i>S.</i> <i>pneumoniae</i>	(36)
<i>P. taiwanensis</i>		
VLB120	wild type	Prof. Dr. A. Schmid (UFZ, Leipzig, DE)
VLB120 pSTY ⁻	VLB120 devoid of megaplasmid pSTY	(29)
VLB120 Δ <i>ndh1</i>	Δ <i>ndh1</i> (PVLB_13270), pSTY ⁻	This study
VLB120 Δ <i>ndh2</i>	Δ <i>ndh2</i> (PVLB_21880), pSTY ⁻	This study
VLB120 ΔΔ <i>ndh</i>	ΔΔ <i>ndh</i> (PVLB_13270, PVLB_21880), pSTY ⁻	This study
VLB120 Δ <i>nuo</i>	Δ <i>nuo</i> (PVLB_15600-15660), pSTY ⁻	This study
VLB120 Δ <i>nuo</i> Δ <i>ndh1</i>	Δ <i>ndh1</i> (PVLB_13270), Δ <i>nuo</i> (PVLB_15600-15660), pSTY ⁻	This study
VLB120 pS2311·Nox	Km ^r , VLB120 bearing pS2311·Nox	

VLB120 $\Delta\Delta ndh$
pS2311·Nox

Km^r, $\Delta\Delta ndh$ (PVLB_13270,
PVLB_21880), pSTY^r bearing
pS2311·Nox

This study

894 ^a Gm^r, Km^r, gentamycin, kanamycin resistance, respectively.

895

896 **Table 5.** Primers used in this study.

Primer	Sequence (5' - 3') ^a	Description
SN019	<u>gataacagggtaatctgCGCAGGATGAAAGCTAAACC</u>	TS1 ndh1 forward
SN020	<u>aacagccaTGAGTCGTTCTGAATAACTAC</u>	TS1 ndh1 reverse
SN021	<u>acgactcaTGGCTGTTTCAGCAATGATGG</u>	TS2 ndh1 forward
SN022	<u>cgggtaccgagctcgGCAAGGGCGAGCATGATGAC</u>	TS2 ndh1 reverse
SN023	<u>gataacagggtaatctgTCGACCTCAACACGCACTTC</u>	TS1 ndh2 forward
SN024	<u>ccggcaagCGATGCGATGAGTCATGG</u>	TS1 ndh2 reverse
SN025	<u>tcgcatcgCTTGCCGCGGATAAAGCCAG</u>	TS2 ndh2 forward
SN026	<u>cgggtaccgagctcgCGGCACTCCCAGATAACTTG</u>	TS2 ndh2 reverse
SN027	ATACGGGCCGTTTCATCAGTC	Verification cointegration ndh1 forward
SN028	GCGATCTTGCGAATGGTGTC	Verification cointegration ndh1 reverse
SN029	CCGGCTGAATGACGAATG	Verification cointegration ndh2 forward
SN030	gttacgacccggtgatg	Verification cointegration ndh2 reverse
SN112	<u>tcagataactTTAAGTAGAGCGGCGACTTG</u>	TS1 nuo reverse
SN113	<u>agggataacagggtaatctgCCTTATCGCCGCCGAATCAC</u>	TS1 nuo forward
SN114	<u>ctctacttaaAGTTATCTGAACGGGCTTGG</u>	TS2 nuo forward
SN115	<u>atccccgggtaccgagctcgGCGCTCCAGTTGGTGGATTC</u>	TS2 nuo reverse
SN116	CTCGTCCAAGCCACCTGATG	Verification cointegration nuo forward
SN117	AGCCTCAAGGTCATGGTCTG	Verification cointegration nuo reverse
SN171	CGGACACAGACCATGCATAC	Verification cointegration, binding in <i>nuoA</i>
SN200	CTGCACACCTATGCCTACAA	qPCR ndh2 forward
SN201	TACAGCGACACATAGAACATCC	qPCR ndh2 reverse
SN214	TTGGCCCAGAGGAAATCAC	qPCR rpoB forward
SN215	GGCACCGACGTAGACAATAC	qPCR rpoB reverse
SN234	AGAACGAACCCTTCGAATCC	qPCR nuoA forward
SN235	GCATCGCGACCAGATAGAAT	qPCR nuoA reverse
SN228	CGAATACGTCGCTAGCCATAC	qPCR ndh1 forward
SN229	ATCACTTTCAGGTGCTCGTC	qPCR ndh1 forward

897 ^aUnderlined nucleotides refer to gene-specific regions; the primer efficiency of the qPCR
898 primer pairs for *ndh2* (SN200, SN201), *rpoB* (SN214, SN215), *nuoA* (SN234, SN235),
899 and *ndh1* (SN228 and SN229) was 104.4%, 101.8%, 104.4 % and 103.4%, respectively.
900

901

902